11-2020

Strain and Stress Relationships for Optical Phonon Modes in Monoclinic Crystals with β-Ga_2O_3 as an Example

Rafal Korlacki
University of Nebraska-Lincoln, rkorlacki2@unl.edu

Megan Stokey
University of Nebraska-Lincoln, mstokey@huskers.unl.edu

Alyssa Lynn Mock
University of Nebraska - Lincoln, alyssalynnmock@gmail.com

Sean Knight
University of Nebraska-Lincoln, seanknight@unomaha.edu

Alexis Papamichail
Linköping University

See next page for additional authors

Rapid Communications

Strain and stress relationships for optical phonon modes in monoclinic crystals with β-Ga_2O_3 as an example

R. Korlacki,[1,*] M. Stokey,[1] A. Mock,[2] S. Knight,[1] A. Papamichail,[3] V. Darakchieva,[3] and M. Schubert[1,3,4,†]

[1]*Department of Electrical and Computer Engineering, University of Nebraska-Lincoln, Lincoln, Nebraska 68588, USA*

[2]*NRC Research Associateship Programs, 500 Fifth Street, Washington, DC 20001, USA*

[3]*Terahertz Materials Analysis Center and Competence Center for III-Nitride Technology C3NiT–Janzén, Department of Physics, Chemistry and Biology (IFM), Linköping University, Linköping SE 58183, Sweden*

[4]*Leibniz Institute for Polymer Research, Dresden D-01069, Germany*

(Received 27 May 2020; revised 27 October 2020; accepted 29 October 2020; published 12 November 2020)

Strain-stress relationships for physical properties are of interest for heteroepitaxial material systems, where strain and stress are inherent due to thermal expansion and lattice mismatch. We report linear perturbation theory strain and stress relationships for optical phonon modes in monoclinic crystals for strain and stress situations which maintain the monoclinic symmetry of the crystal. By using symmetry group analysis and phonon frequencies obtained under various deformation scenarios from density-functional perturbation theory calculations on β-Ga_2O_3, we obtain four strain and four stress potential parameters for each phonon mode. We demonstrate that these parameters are sufficient to describe the frequency shift of the modes regardless of the stress or strain pattern which maintain the monoclinic symmetry of the crystal. The deformation potentials can be used together with experimentally determined phonon frequency parameters from Raman or infrared spectroscopy to evaluate the state of strain or stress of β-Ga_2O_3, for example, in epitaxial heterostructures.

DOI: 10.1103/PhysRevB.102.180101

The state of strain and its resulting stress imposes characteristic modifications to fundamental physical properties, such as electronic structure and phonons of solid state matter. Relationships for, e.g., band-gap energies, electronic states, and phonon modes are of fundamental interest for heteroepitaxial material systems, where strain and stress are inherent due to thermal expansion and lattice mismatch. Strain/stress leads to deviation of the lattice parameters from their equilibrium position. A range of lattice parameter deviations exists within which the strain/stress-induced modifications of the electronic and vibrational states can be described as first-order (linear) perturbations of the quantum states of the strain-free crystal. It is convenient to express the strain/stress induced modifications using deformation potentials, which are defined from joint considerations of group theory and quantum mechanics by application of the theory of invariants for the specific crystal lattice [1]. Knowledge of deformation potentials is put to use to determine accurately and precisely the state of strain or stress by measuring, for example, changes in phonon mode frequencies in comparison with shifts calculated using deformation potentials and thereby identifying the strain/stress parameters existent with the sample under investigation. For many decades, group-theoretic methods have provided useful insights into strain-induced modifications of crystal band structure related properties [1]. Experimentally, deformation potentials can be determined by combining optical spectroscopic techniques to assess the optical and vibration modes and x-ray diffraction measurements of lattice parameters.

Strain and stress relationships for phonons in materials with high crystal symmetry have been extensively investigated. In a seminal work, Tekippe *et al.* demonstrated the use of perturbation theory utilizing deformation potentials linear in strain and group theory to identify deformation potential constants for the effect of uniaxial stress on the Raman-active modes of α-quartz (trigonal, space group $P3_221$) [2]. Briggs and Ramdas later extended the concept for Raman- and infrared-active modes of CdS (hexagonal, space group $P6_3mc$) under uniaxial stress [3]. Since then, significant research efforts have been devoted to establishing the deformation potentials of Raman- and infrared-active phonons in the area of heteroepitaxy of, for example, diamond-structure (e.g., Si, Ge, GeSn, cubic ZrO) [4–10], zinc-blende structure (e.g., GaAs, InSb, CdTe, $In_{1-x}Ga_xAs$) [11–14], cubic tetrahedrally bonded (e.g., BN, AlN, GaN, InN) [15,16], wurtzite-structure (e.g., BN AlN, GaN, InN, ZnO) [16–35], hexagonal (e.g., SiC) [36], corundum-structure (e.g., sapphire) [37], perovskite-structure (e.g., $PbZrTiO_3$, $BaTiO_3$) [38,39], and trigonal symmetry (e.g., $LiNbO_3$) [40] semiconductors.

Notably, monoclinic symmetry β-Ga_2O_3, a new ultrawide band-gap material, has attracted significant research attention due to its high potential for high-power switching devices for a sustainable energy economy [41]. In addition, β-Ga_2O_3 is very promising for harsh environment electronics and for optoelectronic applications in the deep ultraviolet spectral range [42–44]. Strain effects are very important in

*rkorlacki2@unl.edu

†schubert@engr.unl.edu; http://ellipsometry.unl.edu

TABLE I. Character table for the monoclinic group C_{2h}.

	E	C_2	I	σ_h
A_g	1	1	1	1
B_g	1	−1	1	−1
A_u	1	1	−1	−1
B_u	1	−1	−1	1

heterostructures of β-Ga_2O_3 and its alloys with Al_2O_3 and In_2O_3, envisioned as key components of next-generation electronic devices. In contrast to the extensive investigations of high-symmetry crystalline materials, no theoretical and no experimental studies on the strain-stress relationships of Raman- and infrared-active phonons in crystals with monoclinic symmetry can be found in the literature presently. Therefore, in this work, we report the linear perturbation theory strain and stress relationships for infrared- and Raman-active phonon modes in crystals with monoclinic (C_{2h}) symmetry for strain and stress situations which maintain the monoclinic symmetry of the crystal, and we determine the strain and stress deformation potentials using density-functional perturbation theory (DFPT) calculations for β-Ga_2O_3 as an example.

The symmetry of a crystal under a general stress is determined by the symmetry elements common to both the unstrained crystal and the symmetry elements of the strain and the stress tensors [3,45]. We use linear perturbation theory [2], and derive simple relationships between phonon mode energies and the strain/stress parameters for a monoclinic crystal under strain/stress. The symmetry of a crystal under a general strain/stress is determined by the symmetry elements common to both the unstrained crystal and the symmetry elements of the strain/stress tensors [3,45]. Here we consider only strain/stress which does not change the symmetry of the crystal. We consider a usual quantum system $H|S_n\rangle = E_n|S_n\rangle$, where H, $|S_n\rangle$, and E_n are Hamiltonian operator, its nth eigenstate (here: phonon mode), and eigenenergy (here: phonon energy), respectively. A small perturbation, $\delta H_n|S_n\rangle = \Delta E_n|S_n\rangle$ causes an energy shift ΔE_n, which follows from the secular equation, $\sum_{ij}^{N}(\{V_n\}_{ij} - \Delta E_n\delta_{ij}) = 0$. The operator δH_n is related to the nth eigenstate. The matrix $\{V_n\}_{ij} = \langle u_i|\delta H_n|u_j\rangle$ contains the deformation potentials obtained by the usual bracket operations, $|u_i\rangle$ and $\langle u_i|$ are the usual *ket* and *bra* notations of a complete set of functions with dimension N sufficient to describe all states of the quantum system, and δ_{ij} is the Kronecker symbol. The irreducible Γ-point representation for optical phonon modes in β-Ga_2O_3 is $10A_g + 4A_u + 5B_g + 8B_u$. Modes A_g and B_g are Raman active, and modes A_u and B_u are infrared active. Table I lists the characters of all modes. We seek to construct the matrix $\{V_n\}_{ij}$ by using symmetry considerations. We show here for demonstration the case of strain (for stress, replace ϵ with σ). We require that, by first-order Taylor expansion, functionals in δH_n factorize with the monoclinic strain/stress tensor elements

$$\delta H_n = \delta H_0 + \left\{v_n^{xx}\epsilon_{xx}, v_n^{xy}\epsilon_{xy}, v_n^{yy}\epsilon_{yy}, v_n^{zz}\epsilon_{zz}\right\}, \tag{1}$$

where we introduce by writing functionals v_n^{xx}, v_n^{xy}, v_n^{yy}, v_n^{zz}, and δH_0 is dropped since it does not affect ΔE_n. The brackets $\{\cdot\}$ indicate certain yet unknown arrangements of functionals within a representation of the operator δH_n. Seeking a matrix representation, the dimension and structure of the Hilbert space for δH_n can be constructed with the help of a dyadic representation,

$$\delta H_n = v_n \otimes \epsilon, \tag{2}$$

where v_n contains functionals and $\otimes$ is the Kronecker product. The solutions to the secular equation must contain terms represented by basis functions. At least third-order basis functions are needed to render elements in Eq. (2) when v_n represents a rank one dyadic, and fourth-order basis functions are needed when v_n represents a rank two dyadic.

For the Raman-active modes, third-order functions do not exist (see Table II). Hence, representation of Eq. (2) requires fourth-order basis functions, hence

$$\delta H_{A_g} = \begin{bmatrix} a' & a'' & 0 \\ a'' & a''' & 0 \\ 0 & 0 & a'''' \end{bmatrix} \otimes \begin{bmatrix} \epsilon_{xx} & \epsilon_{xy} & 0 \\ \epsilon_{xy} & \epsilon_{yy} & 0 \\ 0 & 0 & \epsilon_{zz} \end{bmatrix}, \tag{3}$$

$$\delta H_{B_g} = \begin{bmatrix} 0 & 0 & u' \\ 0 & 0 & u'' \\ u' & u'' & 0 \end{bmatrix} \otimes \begin{bmatrix} \epsilon_{xx} & \epsilon_{xy} & 0 \\ \epsilon_{xy} & \epsilon_{yy} & 0 \\ 0 & 0 & \epsilon_{zz} \end{bmatrix}, \tag{4}$$

where a', a'', a''', a'''' and u', u'' represent sets of functionals v^{ij}. For the infrared-active modes, third-order functions exist (see Table II), hence

$$\delta H_{A_u} = [\tilde{a}] \otimes \begin{bmatrix} \epsilon_{xx} & \epsilon_{xy} & 0 \\ \epsilon_{xy} & \epsilon_{yy} & 0 \\ 0 & 0 & \epsilon_{zz} \end{bmatrix}, \tag{5}$$

$$\delta H_{B_u} = [\tilde{u}] \otimes \begin{bmatrix} \epsilon_{xx} & \epsilon_{xy} & 0 \\ \epsilon_{xy} & \epsilon_{yy} & 0 \\ 0 & 0 & \epsilon_{zz} \end{bmatrix}, \tag{6}$$

where $\tilde{a}$ and $\tilde{u}$ represent sets of functionals v^{ij}. We note that $[\tilde{a}]$ transforms as (x, y) and $[\tilde{u}]$ transforms as (z) under symmetry operations in Table I. It can be easily seen that all matrices δH_n above transform with the respective character for

TABLE II. Basis functions for irreducible representation C_{2h}, where $\star$ indicates all possible combinations of products between elements of the first parentheses with elements of the second parentheses.

Order	First	Second	Third	Fourth
A_g	R_z	x^2, y^2, z^2, xy		$(x^2, y^2, z^2, xy) \star (x^2, y^2, z^2, xy)$
B_g	R_x, R_y	xz, yz		$(xz, yz) \star (x^2, y^2, z^2, xy)$
A_u	z		$(z) \star (x^2, y^2, z^2, xy)$	
B_u	$x,\ y$		$(x, y) \star (x^2, y^2, z^2, xy)$	

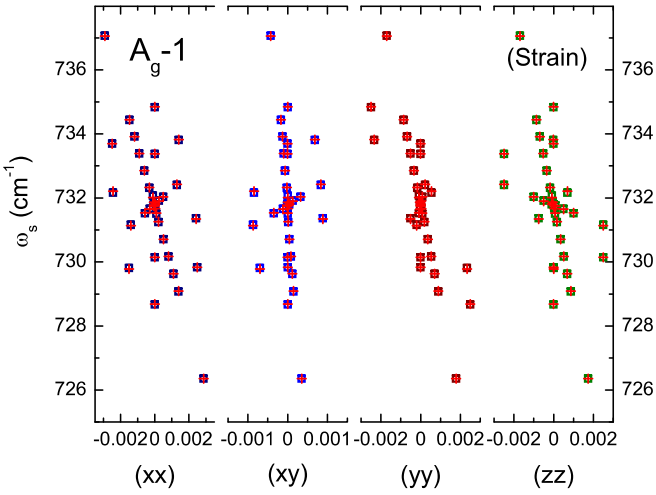

FIG. 1. DFPT-derived (squares) and best-match linear strain deformation potentials calculated (crosses) frequencies for mode A_g-1 versus strain tensor elements ϵ_{xx}, ϵ_{xy}, ϵ_{yy}, and ϵ_{zz} under various deformations (see text).

every mode as indicated in Table I. The expansion of δH_n and its corresponding coefficient matrix $\{V_n\}_{ij}$ is shown and discussed in more detail in the Supplemental Material [46]. For the Raman- and infrared-active modes, $\{V_n\}_{ij}$ is a 9×9 and 3×3 dyadic, respectively, where the Kronecker product in Eq. (2) identifies structure and location of coefficients within $\{V_n\}_{ij}$. The eigenvalues of $\{V_n\}_{ij}$ then provide the solutions. We further require that coefficients with higher orders in the strain/stress parameters vanish. Thereby, we obtain a linear relationship for all modes with all strain parameters

$$\Delta E_n = P_{n,xx}\epsilon_{xx} + P_{n,yy}\epsilon_{yy} + P_{n,zz}\epsilon_{zz} + P_{n,xy}\epsilon_{xy}, \qquad (7)$$

where $P_{n,ij} = \langle S_n | v^{ij} | S_n \rangle$ are the strain deformation potentials, with $n \in \{A_g, B_g, A_u, B_u\}$ and $ij \in \{xx, xy, yy, zz\}$. Hence, four strain ($P_{n,ij}$) and four stress deformation potentials ($\tilde{P}_{n,ij}$) are required for every phonon mode to calculate its energy shift, ΔE_n for small strain/stress parameters. For β-Ga_2O_3, for $10A_g$, $4A_u$, $5B_g$, and $8B_u$ modes 216 potential parameters exist,

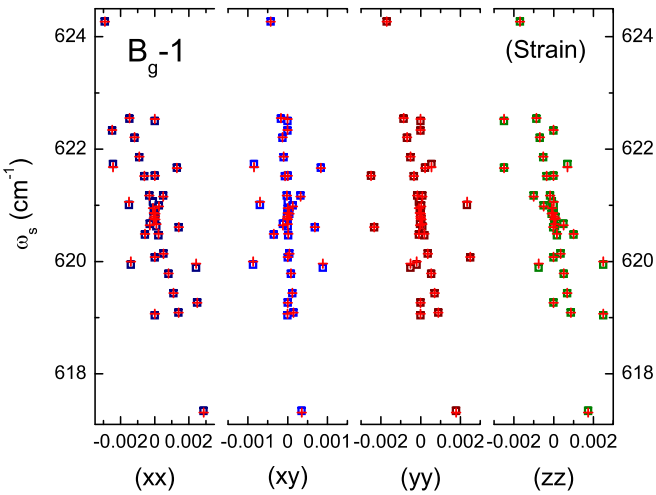

FIG. 2. Same as Fig. 1 for mode B_g-1.

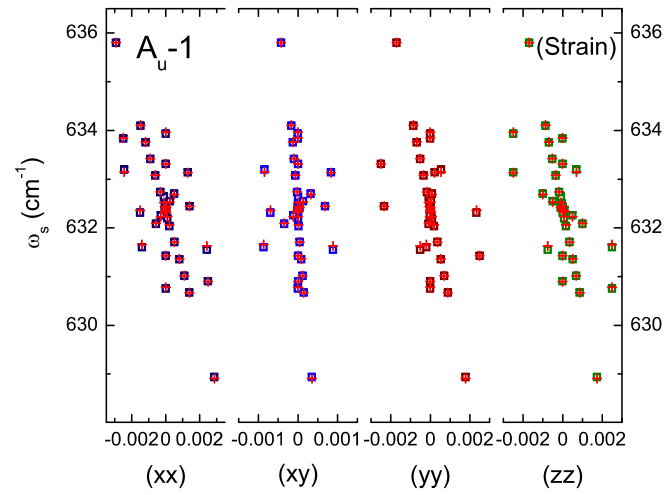

FIG. 3. Same as Fig. 1 for mode A_u-1.

and none have been reported so far from experiment. We note that we only calculated here the potential parameters for the transverse optical IR-active modes, and 48 additional potential parameters exist for the longitudinal optical modes.

A series of DFPT calculations of phonon mode frequencies for β-Ga_2O_3 under different deformation scenarios were performed. We have recently reported on strain-free phonon mode properties in β-Ga_2O_3 [47–49]. A definition of the unit cell, crystal axes, and coordinate system for β-Ga_2O_3 is given in the Supplemental Material. Here, we used the plane-wave code QUANTUM ESPRESSO [50] with a combination of generalized-gradient-approximation density functional of Perdew, Burke, and Ernzerhof [51] and norm-conserving Troullier-Martins pseudopotentials originally generated using FHI98PP [52,53] available in the QUANTUM ESPRESSO pseudopotentials library. The pseudopotential for gallium did not include the semicore $3d$ states in the valence configuration. In order to minimize the impact of Pulay stresses and to ensure numerical convergence of phonon frequencies to at least < 0.1 cm^{-1}, all calculations were performed with a very high electronic wave-function cutoff of 400 Ry, and a dense shifted $8 \times 8 \times 8$ Monkhorst-Pack [54] grid for sampling of the Brillouin zone. A convergence threshold of 1×10^{-12} Ry was used to reach self-consistency. We considered a range of different deformation scenarios: hydrostatic pressure (with equal diagonal components of the stress tensor); uniaxial stress (with a single nonzero component of the stress tensor); and uniaxial strain (with a single nonzero component of the strain tensor). In all scenarios we ensured that the symmetry of the monoclinic cell was not further reduced to triclinic, i.e., all deformation scenarios studied did not induce shear stresses and/or shear strains involving the monoclinic axis b. All structures were relaxed with tight convergence thresholds of 1×10^{-6} Ry for energy and 1×10^{-5} Ry/bohr for forces. The case of hydrostatic pressure was obtained by setting the target pressure during the structural relaxation as implemented in the code. The case of uniaxial stress was obtained by varying the length of one principal lattice vector at a time (or lattice vector component in the case of **c**) followed by a constrained structural relaxation, during which the element initially strained was kept constant and all the remaining cell

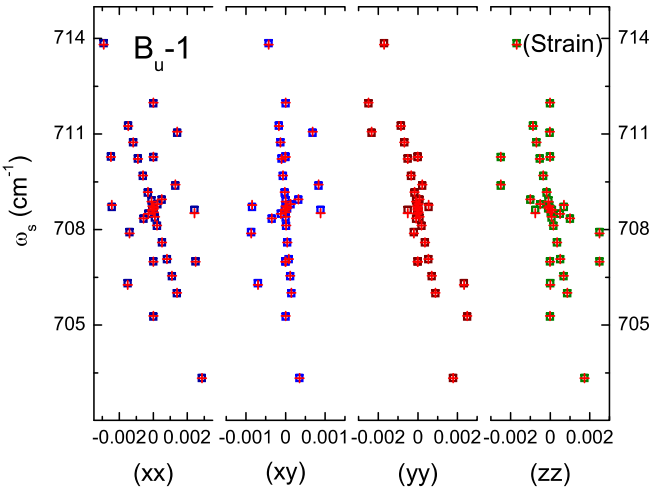

FIG. 4. Same as Fig. 1 for mode B_u-1.

parameters were allowed to relax. During such a constrained structural relaxation, all stress tensor elements except one diagonal component relaxed to zero. This procedure is described in greater detail in the Supplemental Material. Finally, for the case of uniaxial strain we adapted half of the structures that the Thermo_pw code [55] uses to compute the complete elastic tensor, which is described in the Supplemental Material. In short, a simple strain tensor with a single nonzero diagonal component was applied to each lattice vector, followed by a relaxation of ionic positions in a fixed strained cell. In all deformation scenarios we rely on the stress tensor values printed by the code (QE). It is worth noting here that in the case of uniaxial stress, the simple uniaxial stress tensor is a result of constrained structural relaxation and the resulting strain tensor is not simple, as all unit cell parameters differ from their equilibrium values. In contrast, in the case of uniaxial strain, the initial simple single-component strain tensor does not change during the ionic relaxation, while the resulting stress tensor has nonzero values of all four of its independent components. All the fully relaxed cells were used for subsequent DFPT phonon calculations [56], as implemented in the code (QE), with the convergence threshold for self-consistency of 1×10^{-18} Ry. The lattice parameters for all structures included in the present study, and the corresponding phonon frequencies, are provided in the Supplemental Material.

Figures 1–4 depict DFPT-derived frequencies for the A_g-1, B_g-1, A_u-1, and B_u-1 phonon modes versus strain tensor elements, respectively. Thereby, a four-dimensional data set is obtained with either strain or stress tensor elements as base. Hence, each figure contains four panels, where the frequencies are plotted versus one of the strain tensor elements. Note that in order to present the four-dimensional

TABLE III. DFPT-derived frequency (ω_0), linear strain ($P_{\eta,...}$), and stress ($\tilde{P}_{\eta,...}$) potentials for phonon modes in β-Ga_2O_3 in units of cm^{-1}, cm^{-1}/(unit strain), and cm^{-1}/kbar, respectively. The permitted maximum strain was limited to ± 0.0035. The maximum permitted stress was limited to ± 12.5 kbar.

Mode	ω_0	$P_{\eta,xx}$	$P_{\eta,xy}$	$P_{\eta,yy}$	$P_{\eta,zz}$	$\tilde{P}_{\eta,xx}$	$\tilde{P}_{\eta,xy}$	$\tilde{P}_{\eta,yy}$	$\tilde{P}_{\eta,zz}$
A_u-1	632.4	−589	−27	−376	−637	0.217	0.095	0.012	0.118
A_u-2	431.4	−28	137	−773	−570	−0.263	−0.121	0.297	0.208
A_u-3	293.7	−485	−5	−351	−967	0.109	0.164	0.009	0.246
A_u-4	148.6	43	62	−116	−9	−0.067	−0.073	0.059	0.017
B_u-1	708.6	−658	342	−1339	−658	0.037	−0.049	0.376	0.111
B_u-2	659.2	−886	98	−614	−983	0.311	0.109	0.033	0.182
B_u-3	536.2	−1155	422	−1270	−733	0.371	−0.085	0.244	0.046
B_u-4	410.3	−952	−58	−550	−255	0.541	0.406	−0.015	−0.115
B_u-5	343.5	−301	11	−402	−489	0.050	0.113	0.079	0.108
B_u-6	266.3	−309	236	−283	−254	0.051	−0.294	0.066	0.054
B_u-7	248.6	−402	47	−34	−306	0.211	0.003	−0.075	0.037
B_u-8	195.9	547	−163	122	301	−0.257	−0.201	0.057	−0.023
A_g-1	731.7	−773	384	−1239	−656	0.122	−0.132	0.317	0.095
A_g-2	624.6	−939	223	−871	−1006	0.335	0.049	0.129	0.068
A_g-3	596.7	−996	151	−805	−1014	0.346	0.126	0.080	0.165
A_g-4	458.3	−705	111	−770	−403	0.263	0.169	0.136	−0.002
A_g-5	396.9	−115	176	−505	−140	−0.068	−0.077	0.170	0.033
A_g-6	333.0	−619	209	−735	−822	0.098	−0.092	0.155	0.185
A_g-7	303.4	−488	95	−454	−126	0.226	0.091	0.066	−0.053
A_g-8	188.5	−189	176	−404	−285	−0.042	−0.202	0.128	0.081
A_g-9	160.7	−185	114	−149	−75	0.061	−0.106	0.026	0.010
A_g-10	106.7	20	−34	−89	−57	−0.028	0.083	0.033	0.017
B_g-1	620.8	−615	−11	−289	−694	0.245	0.131	−0.030	0.132
B_g-2	458.5	−309	178	−852	−635	−0.111	−0.081	0.267	0.181
B_g-3	344.1	−644	133	−249	676	0.268	−0.028	−0.049	0.124
B_g-4	140.1	−182	95	−287	−372	−0.012	−0.051	0.071	0.105
B_g-5	109.7	10	−67	154	156	0.067	0.0774	−0.062	−0.060

data set, for every data point $\{\omega_s, (xx, yy, zz, xy)\}$, the same frequency is plotted four times, once versus each of its strain coordinates. The data set comprises DFPT calculations with various scenarios of different hydrostatic stress, uniaxial stress, and uniaxial strain. We have included all available data points (provided explicitly in the Supplemental Material), and thereby different slopes appear because of the mixed strain parameter situations. Nonetheless, the four deformation potential parameters still reproduce all DFPT calculated data. Frequencies for all modes versus stress tensor elements are also shown within the Supplemental Material. Included in Figs. 1–4 are the results from a best-match model analysis using Eq. (7) with four deformation potentials. In our best-match model analysis, we limited the permissible strains (stresses) to a maximum of ± 0.0035 (± 12.5 kbar). At higher values, lattice deformations lead to nonlinear changes of the phonon mode frequencies, which cannot be described by our linear deformation theory model. Within the permissible strain/stress values, the DFPT-calculated phonon frequencies show a linear shift. All frequencies were analyzed using Eq. (7), and the resulting deformation potentials are listed in Table III. The strain-free values ω_0 are consistent with those reported by us recently [49]. It is worth noting that while some of the phonon modes exhibit very little sensitivity to an external perturbation, the frequencies of some phonon modes shift significantly as reflected by the large absolute values of the potentials in Table III. In particular, IR-active modes B_u-1, B_u-2, and B_u-3 as well as Raman-active modes A_g-1 to A_g-4, and A_g-6 could be identified as potential candidates for estimating strain in epitaxial films and device heterostructures.

In summary, we have presented the effects of symmetry-conserving lattice deformations in linear approximation onto the phonon modes in monoclinic symmetry crystals using a group-theory analysis, and we have determined the strain and stress deformation potentials by density-functional perturbation theory calculations for monoclinic β-Ga_2O_3. We conclude that the group-theoretical approach we presented here leads to correct and thereby valuable parametrization of phonon modes in monoclinic symmetry crystals, and we anticipate its use for determination of strain and stress in heterostructures for future electronic materials such as β-Ga_2O_3 and related alloys.

This work was supported in part by the National Science Foundation under Award No. DMR 1808715, by Air Force Office of Scientific Research under Award No.FA9550-18-1-0360, by the Nebraska Materials Research Science and Engineering Center under Award No.DMR 1420645, the Swedish Governmental Agency for Innovation Systems (VINNOVA) under the Competence Center Program Grant No. 2016-05190, the Swedish Research Council VR Award No. 2016-00889, the Swedish Foundation for Strategic Research Grants No. RIF14-055 and No. EM16-0024, by the Knut and Alice Wallenberg Foundation supported grant "Wide-bandgap semiconductors for next generation quantum components," and by the Swedish Government Strategic Research Area in Materials Science on Functional Materials at Linköping University, Faculty Grant SFO Mat LiU No. 2009-00971. M.S. acknowledges the University of Nebraska Foundation and the J. A. Woollam Foundation for financial support. This research was performed with support to A.M. from an NRC Research Associateship award at the U.S. Naval Research Laboratory. DFT calculations were in part performed at the Holland Computing Center of the University of Nebraska, which receives support from the Nebraska Research Initiative. The authors gratefully acknowledge a thorough reading of the manuscript and many insightful comments by the reviewer.

[1] L. G. Bir and G. E. Pikus, *Symmetry and Strain-Induced Effects in Semiconductors* (Wiley, New York, 1974).
[2] V. J. Tekippe, A. K. Ramdas, and S. Rodriguez, Phys. Rev. B **8**, 706 (1973).
[3] R. J. Briggs and A. K. Ramdas, Phys. Rev. B **13**, 5518 (1976).
[4] S. J. Harris, A. E. O'Neill, W. Yang, P. Gustafson, J. Boileau, W. H. Weber, B. Majumdar, and S. Ghosh, J. Appl. Phys. **96**, 7195 (2004).
[5] E. Anastassakis, Solid State Commun. **84**, 47 (1992).
[6] E. Anastassakis, Philos. Mag. B **70**, 359 (1994).
[7] A. Gassenq, S. Tardif, K. Guilloy, I. Duchemin, N. Pauc, J. M. Hartmann, D. Rouchon, J. Widiez, Y. M. Niquet, L. Milord, T. Zabel, H. Sigg, J. Faist, A. Chelnokov, F. Rieutord, V. Reboud, and V. Calvo, J. Appl. Phys. **121**, 055702 (2017).
[8] E. Anastassakis and E. Liarokapis, J. Appl. Phys. **62**, 3346 (1987).
[9] K. Takeuchi, K. Suda, R. Yokogawa, K. Usuda, N. Sawamoto, and A. Ogura, Jpn. J. Appl. Phys. **55**, 091301 (2016).
[10] J. Cai, Y. S. Raptis, and E. Anastassakis, Appl. Phys. Lett. **62**, 2781 (1993).
[11] V. C. Stergiou, N. T. Pelekanos, and Y. S. Raptis, Phys. Rev. B **67**, 165304 (2003).
[12] D. J. Lockwood, G. Yu, N. L. Rowell, and P. J. Poole, J. Appl. Phys. **101**, 113524 (2007).
[13] M. Hünermann, W. Richter, J. Saalmüller, and E. Anastassakis, Phys. Rev. B **34**, 5381 (1986).
[14] M. Siakavellas, Y. S. Raptis, E. Anastassakis, and D. J. Lockwood, J. Appl. Phys. **82**, 6235 (1997).
[15] K. Kim, W. R. L. Lambrecht, and B. Segall, Phys. Rev. B **50**, 1502 (1994).
[16] K. Kim, W. R. L. Lambrecht, and B. Segall, Phys. Rev. B **53**, 16310 (1996).
[17] H. Harima, J. Phys.: Condens. Matter **38**, R967 (2002).
[18] V. Y. Davydov, N. S. Averkiev, I. N. Goncharyk, D. K. Nelson, I. P. Nikitina, A. S. Polkovnikov, A. N. Smirnov, M. A. Jacobson, and O. K. Semchinova, J. Appl. Phys. **82**, 5097 (1997).
[19] C. Kisielowski, J. Krüger, S. Ruvimov, T. Suski, J. W. Ager, III, E. Jones, Z. Liliental-Weber, M. Rubin, E. R. Weber, M. D. Bremser, and R. F. Davis, Phys. Rev. B **54**, 17745 (1996).
[20] T. Kozawa, T. Kachi, H. Kano, and H. Nagase, J. Appl. Phys. **77**, 4389 (1995).
[21] F. Demangeot, J. Frandon, M. A. Renucci, O. Briot, B. Gil, and R. L. Aulombard, Solid State Comput. **100**, 207 (1995).

[22] D. Zhao, S. Xu, M. Xie, S. Tong, and H. Yang, Appl. Phys. Lett. **83**, 677 (2002).

[23] F. Demangeot, J. Frandon, P. Baules, F. Natali, F. Semond, and J. Massies, Phys. Rev. B **69**, 155215 (2004).

[24] V. Darakchieva, T. Paskova, M. Schubert, H. Arwin, P. P. Paskov, B. Monemar, D. Hommel, M. Heuken, J. Off, F. Scholz, B. A. Haskell, P. T. Fini, J. S. Speck, and S. Nakamura, Phys. Rev. B **75**, 195217 (2007).

[25] K. Shimada, T. Sota, and K. Suzuki, J. Appl. Phys. **84**, 4951 (1998).

[26] T. Gruber, G. M. Prinz, C. Kirchner, R. Kling, F. Reuss, W. Limmer, and A. Waag, J. Appl. Phys. **96**, 289 (2004).

[27] J.-M. Wagner and F. Bechstedt, Appl. Phys. Lett. **77**, 346 (2000).

[28] J.-M. Wagner and F. Bechstedt, Phys. Rev. B **66**, 115202 (2002).

[29] J. Gleize, M. A. Renucci, J. Frandon, E. Bellet-Amalric, and B. Daudin, J. Appl. Phys. **93**, 2065 (2003).

[30] A. Sarua, M. Kuball, and J. E. Van Nostrand, Appl. Phys. Lett. **81**, 1426 (2002).

[31] V. Darakchieva, P. Paskov, T. Paskova, J. Birch, S. Tungasmita, and B. Monemar, Appl. Phys. Lett. **80**, 2302 (2002).

[32] G. Callsen, M. R. Wagner, J. S. Reparaz, F. Nippert, T. Kure, S. Kalinowski, A. Hoffmann, M. J. Ford, M. R. Phillips, R. F. Dalmau, R. Schlesser, R. Collazo, and Z. Sitar, Phys. Rev. B **90**, 205206 (2014).

[33] V. Darakchieva, E. Valcheva, P. P. Paskov, M. Schubert, T. Paskova, B. Monemar, H. Amano, and I. Akasaki, Phys. Rev. B **71**, 115329 (2005).

[34] V. Darakchieva, B. Monemar, T. Paskova, S. Einfeldt, D. Hommel, and S. Lourdudoss, Phys. Status Solidi C **4**, 170 (2007).

[35] V. Darakchieva, P. P. Paskov, E. Valcheva, T. Paskova, B. Monemar, M. Schubert, H. Lu, and W. J. Schaff, Appl. Phys. Lett. **84**, 3636 (2004).

[36] R. Sugie and T. Uchida, J. Appl. Phys. **122**, 195703 (2017).

[37] W. Zhu and G. Pezzotti, J. Raman Spectrosc. **42**, 2015 (2011).

[38] M. Deluca and G. Pezzotti, J. Phys. Chem. A **112**, 11165 (2008).

[39] G. Pezzotti, K. Okai, and W. Zhu, J. Appl. Phys. **111**, 013504 (2012).

[40] G. Pezzotti, H. Hagihara, and W. Zhu, J. Phys. D **46**, 145103 (2013).

[41] *Gallium Oxide, Materials Properties, Crystal Growth and Devices*, edited by M. Higashiwaki and S. Fujita (Springer, Switzerland, 2020), Vol. 293.

[42] M. Higashiwaki, K. Sasaki, H. Murakami, Y. Kumagai, A. Koukitu, A. Kuramata, T. Masui, and S. Yamakoshi, Semicond. Sci. Technol. **31**, 034001 (2016).

[43] M. Higashiwaki and G. H. Jessen, Appl. Phys. Lett. **112**, 060401 (2018).

[44] S. J. Pearton, J. Yang, P. H. Cary, F. Ren, J. Kim, M. J. Tadjer, and M. A. Mastro, Appl. Phys. Rev. **5**, 011301 (2018).

[45] H. S. Peiser, J. J. B. Wachtmann, and R. W. Dickinson, J. Res. Natl. Bur. Stand. (USA) **67A**, 395 (1963).

[46] See Supplemental Material at http://link.aps.org/supplemental/10.1103/PhysRevB.102.180101 for the detailed derivation of deformation potentials for monoclinic symmetry, the derivation of monoclinic strain tensor elements, the calculated elastic tensor, a detailed description of obtaining uniaxial stress conditions, and the complete dataset used for the determination of phonon deformation potentials for β-Ga_2O_3. The Supplemental Material includes Refs. [2,3,45,47,57,58].

[47] M. Schubert, R. Korlacki, S. Knight, T. Hofmann, S. Schöche, V. Darakchieva, E. Janzén, B. Monemar, D. Gogova, Q.-T. Thieu, R. Togashi, H. Murakami, Y. Kumagai, K. Goto, A. Kuramata, S. Yamakoshi, and M. Higashiwaki, Phys. Rev. B **93**, 125209 (2016).

[48] M. Schubert, A. Mock, R. Korlacki, and V. Darakchieva, Phys. Rev. B **99**, 041201(R) (2019).

[49] M. Schubert, A. Mock, R. Korlacki, S. Knight, B. Monemar, K. Goto, Y. Kumagai, A. Kuramata, Z. Galazka, G. Wagner, M. Tadjer, V. Wheeler, M. Higashiwaki, and V. Darakchieva, Phonon and free charge carrier properties in monoclinic symmetry gallium oxide, in *Gallium Oxide: Materials Properties, Crystal Growth, and Devices*, edited by M. Higashiwaki and S. Fujita (Springer, New York, 2020), Chap. 28, pp. 501–534.

[50] QUANTUM ESPRESSO is available from http://www.quantum-espresso.org. See also P. Giannozzi, S. Baroni, N. Bonini, M. Calandra, R. Car, C. Cavazzoni, D. Ceresoli, G. L. Chiarotti, M. Cococcioni, I. Dabo *et al.*, J. Phys.: Condens. Matter **21**, 395502 (2009).

[51] J. P. Perdew, K. Burke, and M. Ernzerhof, Phys. Rev. Lett. **77**, 3865 (1996).

[52] M. Fuchs and M. Scheffler, Comput. Phys. Commun. **119**, 67 (1999).

[53] N. Troullier and J. L. Martins, Phys. Rev. B **43**, 1993 (1991).

[54] H. J. Monkhorst and J. D. Pack, Phys. Rev. B **13**, 5188 (1976).

[55] Thermo_pw code is available from https://dalcorso.github.io/thermo_pw/.

[56] S. Baroni, S. de Gironcoli, A. D. Corso, S. Baroni, S. de Gironcoli, and P. Giannozzi, Rev. Mod. Phys. **73**, 515 (2001).

[57] J. Furthmüller and F. Bechstedt, Phys. Rev. B **93**, 115204 (2016).

[58] K. Adachi, H. Ogi, N. Takeuchi, N. Nakamura, H. Watanabe, T. Ito, and Y. Ozaki, J. Appl. Phys. **124**, 085102 (2018).